ACS OMEGA

http://pubs.acs.org/journal/acsodf

Article

Influence of Irradiation Time on the Structural and Optical Characteristics of CuSe Nanoparticles Synthesized via Microwave-Assisted Technique

Ibrahim Garba Shitu, Josephine Ying Chyi Liew,* Zainal Abidin Talib, Hussein Baqiah, Mohd Mustafa Awang Kechik, Mazliana Ahmad Kamarudin, Nurul Huda Osman, Yiin Jian Low, and Ismail Ibrahim Lakin

Cite This: *ACS Omega* 2021, 6, 10698−10708

Read Online

ACCESS | Metrics & More | Article Recommendations

ABSTRACT: A rapid, sustainable, and ecologically sound approach is urgently needed for the production of semiconductor nanomaterials. CuSe nanoparticles (NPs) were synthesized via a microwave-assisted technique using $CuCl_2{\cdot}2H_2O$ and Na_2SeO_3 as the starting materials. The role of the irradiation time was considered as the primary concern to regulate the size and possibly the shape of the synthesized nanoparticles. A range of characterization techniques was used to elucidate the structural and optical properties of the fabricated nanoparticles, which included X-ray diffraction, energy-dispersive X-ray spectroscopy (EDX), atomic force microscopy, field emission scanning electron microscopy, Raman spectroscopy (Raman), UV−Visible diffuse reflectance spectroscopy (DRS), and photoluminescence spectroscopy (PL). The mean crystallite size of the CuSe hexagonal (Klockmannite) crystal structure increased from 21.35 to 99.85 nm with the increase in irradiation time. At the same time, the microstrain and dislocation density decreased from 7.90×10^{-4} to 1.560×10^{-4} and 4.68×10^{-2} to 1.00×10^{-2} nm^{-2}, respectively. Three Raman vibrational bands attributed to CuSe NPs have been identified in the Raman spectrum. Irradiation time was also seen to play a critical role in the NP optical band gap during the synthesis. The decrease in the optical band gap from 1.85 to 1.60 eV is attributed to the increase in the crystallite size when the irradiation time was increased. At 400 nm excitation wavelength, a strong orange emission centered at 610 nm was observed from the PL measurement. The PL intensity is found to increase with an increase in irradiation time, which is attributed to the improvement in crystallinity at higher irradiation time. Therefore, the results obtained in this study could be of great benefit in the field of photonics, solar cells, and optoelectronic applications.

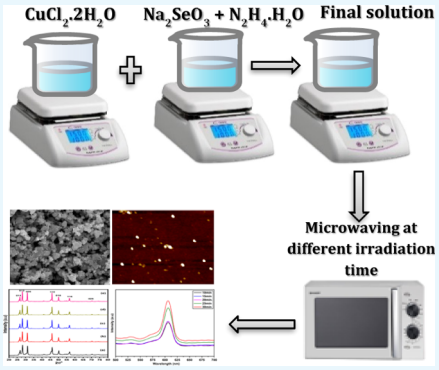

INTRODUCTION

Controlling the size of nanoparticles (NPs) is an essential element to tailor the nanoparticles for specific properties required in applications such as microelectronics, renewable energy, or medicines. In order to realize this, significant steps have been taken to monitor nanoparticle sizes, shapes, and dimensions during fabrication.[1] Recent work has focused on semiconductor nanoparticles owing to their remarkable electronic and optical properties and their wide range of applications, including single-electron transistors,[2] light-emitting diodes,[3] electrochemical nano-sensors,[4] and field-effect thin-film transistors.[5] Various forms of nanoparticles of different sizes and compositions have been used for fabricating and constructing sensors and biosensors. Thus, the size of the nanoparticles has a significant role to play in electrochemical sensing systems.[6] Recently, considerable attention has been given to the preparation and characterization of copper selenide nanoparticles due to their unique properties and potential applications in many fields of science and engineering.[7] Copper selenide has many favorable features when compared with other promising metal selenide semiconductors. It can exist in stoichiometric compositions such as CuSe,[8] Cu_2Se,[9] Cu_3Se_2,[10] $CuSe_2$,[11] and Cu_7Se[12] and non-stoichiometric compositions such as $Cu_{2-x}Se$.[13] More so, the composition exists in diverse crystal structures, such as monoclinic,[14] cubic,[15] tetragonal,[16] and hexagonal.[17] Several approaches have already been used for the synthesis of copper selenides such as mechanical alloy,[18] gamma irradiation,[19] microwave,[20] ultra-sonic synthesis,[21] hydrothermal,[22] sol−

Received: January 9, 2021
Accepted: March 4, 2021
Published: April 12, 2021

https://doi.org/10.1021/acsomega.1c00148
ACS Omega 2021, 6, 10698−10708

gel,[23] solid-state,[24] and chemical reaction solution phase.[25] At the moment, the central focus has turned to the microwave technique to provide the necessary reaction energy required for the synthesis of nanomaterials. This move is in part due to the effective implementation of microwave irradiation in the fields of materials science, nanotechnology, biomedical applications, and organic and inorganic chemistry. Synthesis using microwave irradiation has shown a significant improvement in purity, size, and other properties in the product as compared to traditional heating. Microwave irradiation acts directly upon the mixture content, converting the electromagnetic energy into heat through molecular interactions and thereby generating uniform heat during the synthesis process.[26,27]

The basis for this study is that the conventional method for the synthesis of nanomaterials is not sufficiently fast and ecologically friendly to meet the growing needs for the semiconductor nanomaterials.[28] Scientists are under immense pressure to develop novel methods that are both efficient and do not generate large amounts of hazardous waste. The utilization of water as the solvent in the chemical reaction using microwave irradiation is an alternative. Microwave irradiation has been effective in accelerating the reaction time from days to minutes, which may be decisive to the rapid fabrication of quality nanomaterials in the manufacturing process. Besides, copper selenide preparation methods and size or shape control are less versatile than those of other metal selenides such as CdSe, ZnSe, and FeSe. Studies related to their structural and optical properties are minimal, especially using microwaves as the synthesis technique. Therefore, new methods to prepare and monitor the size and shape of copper selenide nanostructures that are fast and ecologically sound need to be developed.[29,30] To achieve this objective, the chemical reaction to produce CuSe NPs is examined using the microwave-assisted method. The amount of heat channeled to the reaction is varied by changing the irradiation time of the microwave to the solution. The size and shape of the NPs are monitored in order to gather the information that could lead to the design of manufacturing practices for CuSe NPs with specific size and shape. An investigation into the relationship between particle size and shape to the structural and optical properties of the NP semiconductor is also undertaken.

RESULTS AND DISCUSSION

Reaction Mechanism. The mechanism for the reaction to produce the CuSe NPs is described below[31]

$$Na_2SeO_3 \rightarrow Na^+ + SeO_3^{2-} \quad (1)$$

$$N_2H_4{\cdot}2H_2O \rightarrow N_2H_5^+ + OH^- + H_2O \quad (2)$$

$$4SeO_3^{2-} + 5N_2H_5^+ + OH^- \rightarrow 4Se^{2-} + 13H_2O + 5N_2 \quad (3)$$

$$CuCl_2 \rightarrow Cu^{2+} + 2Cl^- \quad (4)$$

$$Cu^{2+} + Se^{2-} \rightarrow CuSe \quad (5)$$

The SeO^{3-} ion was obtained when sodium selenide was added to deionized water and was reduced to the Se^{2-} ion in the presence of hydrazine hydrate. The Se^{2-} ion will then react with the Cu^{2+} ion to form the final product of CuSe NPs.

X-ray Diffraction. Figure 1 presents the X-ray diffraction (XRD) patterns of copper selenide (CuSe) NPs synthesized at different irradiation times. The phase purity and crystalline

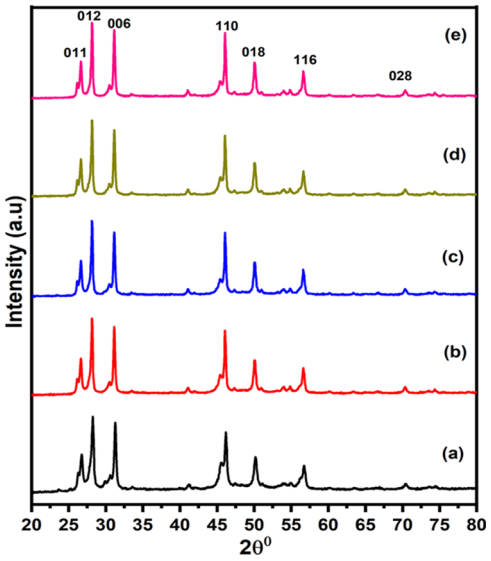

Figure 1. XRD patterns of as-synthesized CuSe NPs at different irradiation times: (a) 10, (b) 15, (c) 20, (d) 25, and (e) 30 min.

structure are observed to be the same for all the synthesized samples. All the XRD patterns show the formation of sharp peaks of single-phase CuSe NPs with diffraction peaks at 2θ values of 26.75, 28.20, 31.50, 45.47, 50.25, 56.85, and 71.20° corresponding to the reflection planes of (011), (012), (006), (110), (018), (116), and (028) respectively. These hkl reflection planes are compatible with the CuSe hexagonal (Klockmannite) structure, which corresponds to ICSD Data File no: 98-004-5640.

It can be seen from the XRD patterns that the full width at half maximum (fwhm) decreases with an increase in irradiation time. The fwhm is closely related to the size of the crystallite of the sample. The narrower the fwhm of the XRD peaks, the larger the size of the crystallite, as illustrated by Sherrer's formula, as shown in eq 6

$$D = \frac{0.94\lambda}{\beta \cos\theta} \quad (6)$$

where λ is the wavelength of the X-ray used, β is the full width at half maximum (fwhm) of a diffraction peak, and θ is Bragg's angle of reflection. Moreover, the microstrain (ε) and dislocation density (δ) of all the samples were obtained using eqs 7 and 8 given below

$$\varepsilon = \frac{\beta \cos\theta}{4} \quad (7)$$

and

$$\delta = \frac{1}{D^2} \quad (8)$$

The estimation of the mean crystallite size of nanostructured materials is usually performed using the famous Debye Scherer formula, which uses the fwhm of the XRD peaks. However, the accuracy of this method is limited when dealing with nanocrystalline materials owing to their considerable peak broadening due to their nanometer size. In many instances, the XRD peak broadening is not only influenced by the nanocrystalline nature of the sample but also affected by the intrinsic strain associated with the as-synthesized sample induced by the crystal imperfections including the point

https://doi.org/10.1021/acsomega.1c00148
ACS Omega 2021, 6, 10698−10708

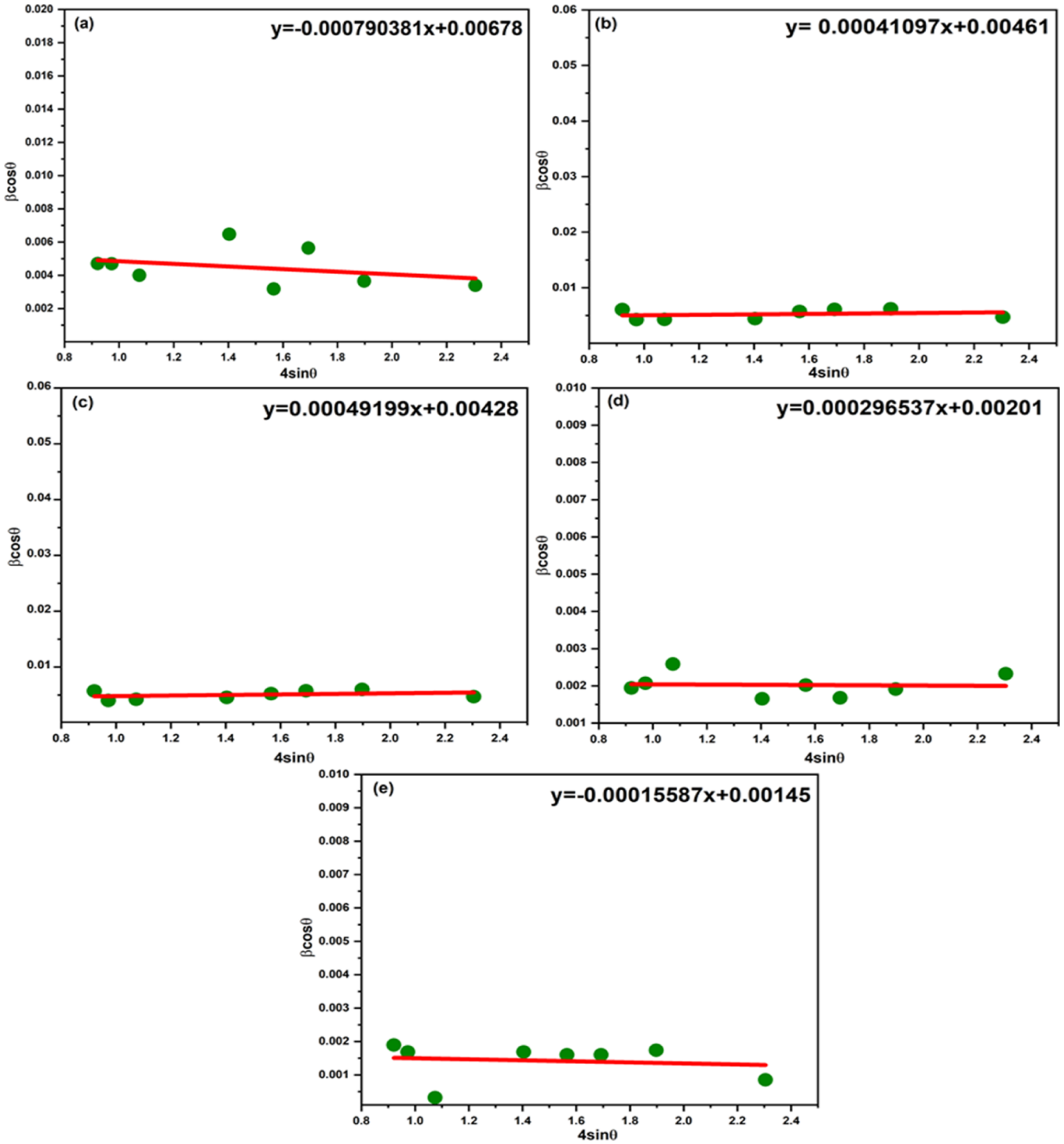

Figure 2. Williamson–Hall plots of CuSe NPs at different irradiation times: (a) 10, (b) 15, (c) 20, (d) 25, and (e) 30 min.

defect, grain boundary, triple junction, and stacking faults in the nanocrystals. For this reason, the Williamson–Hall method was employed to estimate the average crystallite size of all the samples.[32,33] The Williamson–Hall method takes into consideration the width of the diffraction peak as a function of the diffraction angle 2θ. It assumes that the broadening of XRD peaks originates from the small crystallite size and microstrain.[34] The Williamson–Hall equation is given as

$$\beta_{hkl}\cos\theta = \frac{k\lambda}{D} + 4\varepsilon \sin\theta \quad (9)$$

where λ is the wavelength of the X-ray used, k is a constant referred to as a shape factor and usually taken as 0.94, β_{hkl} is the full width at half maximum of the diffraction peaks, θ is Bragg's angle of reflection, D is the average crystallite size, and ε is the intrinsic strain due to crystal imperfection associated with the as-synthesized nanoparticle.

Hence, by plotting a graph of $\beta_{hkl}\cos\theta$ against 4 sin θ for all diffraction planes of CuSe NPs, the crystallite size and the intrinsic strain are obtained from the intercept and the slope of the linearly fitted data, respectively. Figure 2 depicts the Williamson–Hall plots of CuSe NPs synthesized at different

https://doi.org/10.1021/acsomega.1c00148
ACS Omega 2021, 6, 10698–10708

Table 1. Structural Properties of CuSe NPs at Different Irradiation Times

sample designation (min)	crystallite size (nm)		micro-strain (ε) $\times 10^{-3}$		dislocation density (δ) $\times 10^{-3}$ (nm)$^{-2}$	
	Sherrer's method	Williamson–Hall method	Sherrer's method	Williamson–Hall method	Sherrer's method	Williamson–Hall method
10	19.20	21.35	8.22	7.90	2.71	2.20
15	28.40	31.41	5.83	4.11	1.24	1.01
20	30.30	33.83	5.51	4.92	1.09	0.87
25	73.10	72.03	2.68	2.97	0.18	0.19
30	102.40	99.85	2.09	1.56	0.09	0.10

irradiation times. As displayed in Table 1, the mean crystallite size estimated using Scherer's formula are found to increase from 19.20 to 102.40 nm, whereas the microstrain and dislocation density were found to decrease from 8.22×10^{-3} to 2.09×10^{-3} and 2.71×10^{-3} to 9.0×10^{-4}, respectively. However, using the Williamson–Hall method, the average crystallite size is found to increase from 21.35 to 99.85 nm, while the microstrain and dislocation density are found to decrease from 7.90×10^{-4} to 1.56×10^{-4} and 2.20×10^{-3} to 1.00×10^{-4} nm^{-2}, respectively. The mean crystallite sizes estimated using both methods are more or less similar. This implies that the technique used to synthesize the NPs produces a small amount of strain in the product which influences the crystallite size.

Field Emission Scanning Electron Microscopy. Figure 3a presents the field emission scanning electron microscopy (FESEM) images of the as-prepared CuSe NPs synthesized at different irradiation times. The morphology of the as-synthesized CuSe NPs exhibits irregular-shaped particles, which are not evenly distributed. The average particle size is observed to increase with the increase in irradiation time. The mean particle size (Figure 3b) at various irradiation times is found to be 24.18 ± 0.85, 33.80 ± 0.52, 35.42 ± 0.95, 77.23 ± 0.33, and 110.05 ± 0.30 nm corresponding to 10, 15, 20, 25, and 30 min irradiation time, respectively. This finding clearly shows that longer irradiation time has an impact on Ostwald's ripening process due to its influence on interfacial energy, growth rate coefficients, and solubility that can increase particle size.[35] The finding is in good agreement with XRD and AFM results. This observation establishes the role of irradiation time in the synthesis process of the particle size of the CuSe NPs.

Atomic Force Microscopy. Figure 4a exhibits the atomic force microscopy (AFM) images of CuSe NPs synthesized at different irradiation times. Using the UTHSCA image tool, the mean particle size and size distribution of the as-prepared CuSe NPs were evaluated. The mean particle size is found to increase with the increase in irradiation time, as evidently seen from Figure 4b. The average particle size was found to be 21.15 ± 0.21, 30.71 ± 0.15, 32.67 ± 0.35, 74.16 ± 0.92, and 104.89 ± 0.66 nm corresponding to 10, 15, 20 25, and 30 min irradiation time, respectively. The increase in particle size with increasing irradiation time is due to the fact that smaller particles fused into larger ones at higher irradiation times. The formation of CuSe NPs at different microwave irradiation times is owing to the following processes. When the mixture of the precursor's solution is exposed to microwave irradiation, the nucleation processes and growth rate of smaller particles are promoted. The particle size of CuSe NPs increases owing to the Ostwald ripening process over a longer irradiation time. Additionally, the interaction of an electromagnetic field with smaller particles will dissolve and/or deposit smaller particles over the larger ones, which eventually leads to the formation of bigger particles at higher irradiation time.[36] This observation illustrates that varying the microwave irradiation time has an important role in the nucleation process and crystal growth rate, and thus, the average particle size of CuSe NPs was synthesized via a microwave-assisted synthesis method.

Energy-Dispersive X-ray Spectroscopy. Figure 5 presents the energy-dispersive X-ray spectroscopy (EDX) spectrum of the as-synthesized CuSe NPs after being irradiated for 20 min. This X-ray-based analysis yields an accurate account of the elemental composition of the NPs and thus its phase purity. Only peaks assigned to Cu and Se are observed in the synthesized CuSe NPs. The absence of any other peak belonging to other elements in the EDX spectrum indicates that single-phase CuSe NPs have been obtained, which reaffirms the finding of XRD results. Table 2 gives the corresponding atomic weight percentage of the Cu/Se molar ratio of CuSe NPs, which is equivalent to the stoichiometric molar ratio of 1:1 Cu/Se.

Raman Spectroscopy. Raman spectroscopy (RS) investigates the chemical structure of a material by probing the light scattered by the material using a laser.[37] Figure 6 shows the Raman spectrum at the wavelength range of 50–1000 nm of as-synthesized CuSe NPs at 20 min irradiation time (20 min). It is shown that the spectrum consisted of three peaks located at 185.7, 260.2¯, and 510 cm^{-1}. The most intense peak in the spectrum situated at 260 cm^{-1} can be assigned to the first longitudinal optic (LO) phonon mode of Cu–Se vibrations. The two other much weaker peaks situated at 185.7 and 510 cm^{-1} are identified as the transverse optic (TO) and second longitudinal optic (2LO) of the as-synthesized CuSe NPs, respectively.[38] Previous work has observed that the overtones are typically located at frequencies that are double or triple the frequency of the principal peak.[9] Thus, the Raman spectroscopy result is consistent with the previous finding as the first longitudinal overtone (LO) peak for as-synthesized CuSe NPs is detected at nearly two times the frequency of the principal peak.

UV–Visible Diffuse Reflectance Spectroscopy. A room temperature diffuse reflectance spectroscopy (DRS) measurement was conducted on CuSe NPs prepared via a microwave-assisted technique. As-synthesized CuSe NPs show a broad absorption spectrum in the wavelength ranging from 400 to 1000 nm, as depicted in Figure 7. The reflectance values were used to determine the absorption coefficient using the well-known Kubelka–Munk formula as shown in eq 10.

$$F(R_\infty) = \frac{\alpha}{s} = \frac{(1 - R_\infty)}{2R} \tag{10}$$

where α is the absorption coefficient, s is the coefficient of scattering, and $F(R_\infty)$ is the Kubelka–Munk function.[39] In DRS, the Kubelka–Munk function can be used instead of

https://doi.org/10.1021/acsomega.1c00148
ACS Omega 2021, 6, 10698–10708

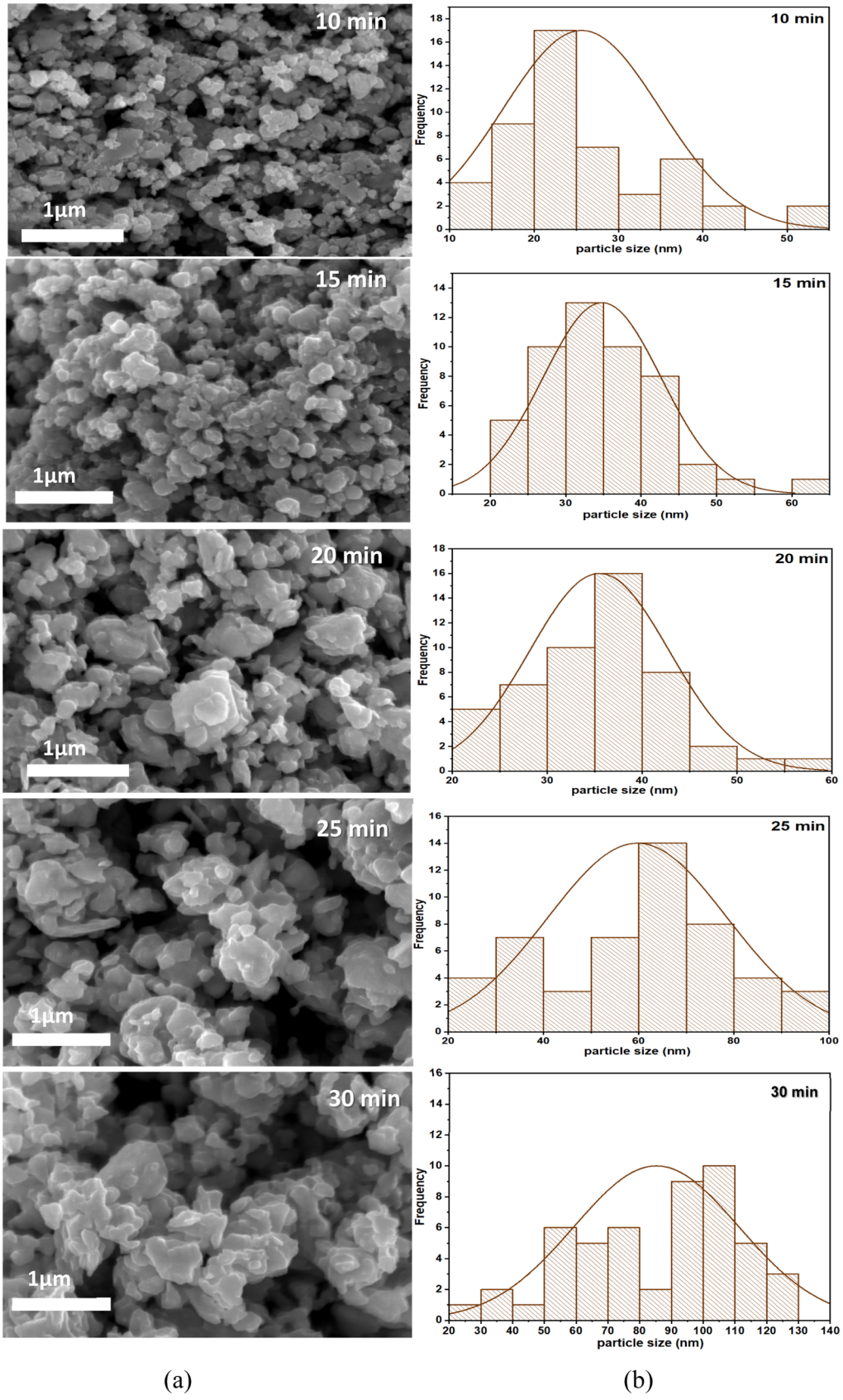

Figure 3. (a) FESEM images and (b) size distribution histograms of CuSe NPs at different irradiation times.

absorbance A to determine the optical absorption edge energy.[40] It is shown that the plot of $[F(R_\infty)E]^{1/n}$ versus E is linear near the edge for a direct transition (n = 1/2). The optical band gap for each sample at different irradiation times is determined using the reflectance spectrum values and using the Kubelka–Munk eq 11

https://doi.org/10.1021/acsomega.1c00148
ACS Omega 2021, 6, 10698−10708

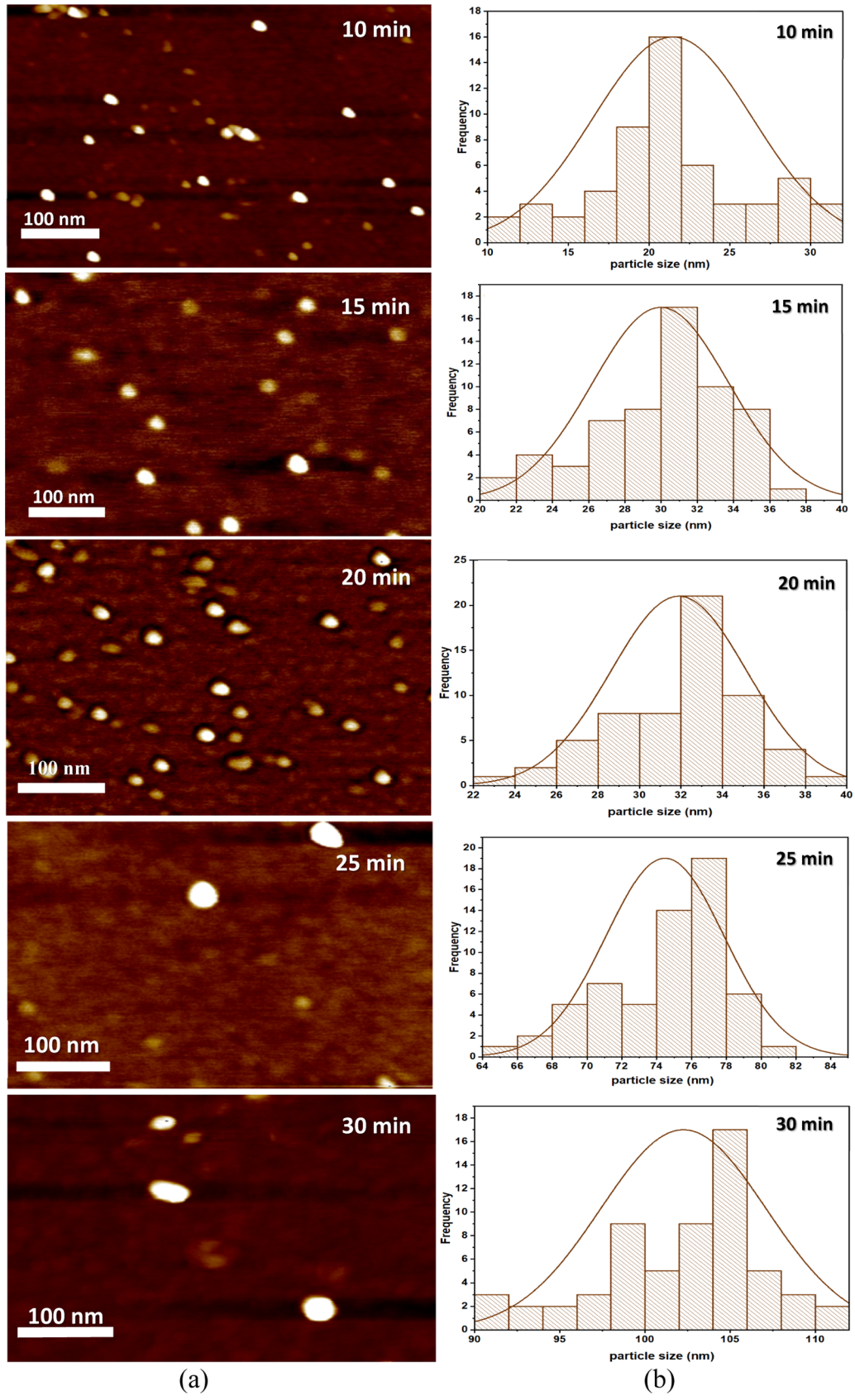

Figure 4. (a) AFM images and (b) size distribution histograms of CuSe NPs at different irradiation times.

$$[F(R_\infty)h\nu)]^2 = A(h\nu - E_g) \quad (11)$$

where $h\nu$ is the incident photon energy and A is the constant based on the diffuse reflectance R_∞ and transition probability. The diffuse reflectance R_∞ is obtained from $R_\infty = R_{Sample}/$

https://doi.org/10.1021/acsomega.1c00148
ACS Omega 2021, 6, 10698−10708

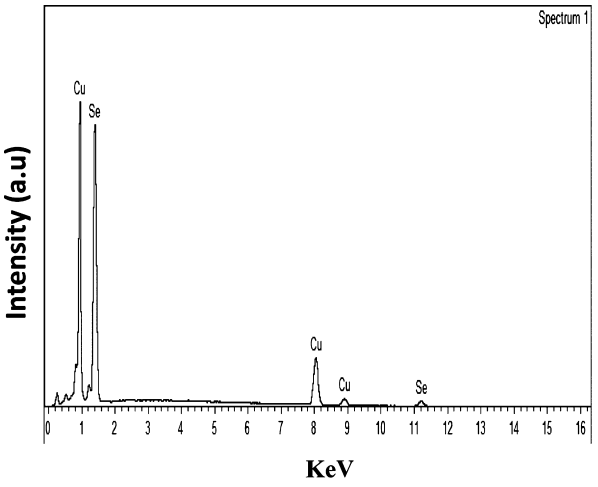

Figure 5. EDX spectrum of as-synthesized CuSe NPs at 20 min irradiation time.

Table 2. Atomic Weight Percentage of Cu/Se from EDX

element	weight %	atomic %
Cu	46.57	51.99
Se	51.58	48.42
total	100	100

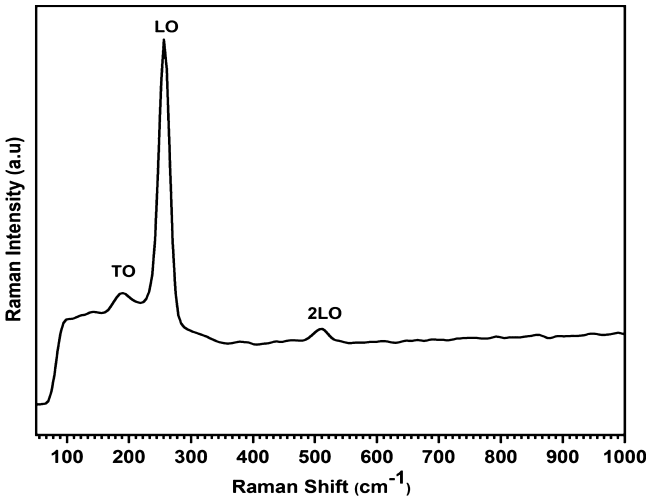

Figure 6. Raman spectrum of as-synthesized CuSe NPs at 20 min irradiation time.

$R_{Standard}$.[41] The plot of $[F(R_\infty)h\nu]^2$ versus $h\nu$ is shown in Figure 8. To determine the optical band gap of the as-prepared CuSe NPs, straight lines are drawn and extended to intersect the $h\nu$ axis as shown in the plots.

It can be seen from Figure 8 that the optical band gap decreases with the increase in irradiation time. The optical band gap is found to decrease from 1.85 to 1.60 eV with the increase in irradiation time, as shown in Table 3. The decrease in the optical band gap with the increase in irradiation time is related to the increase in the particle size of the as-prepared CuSe NPs. The smaller the particle size, the larger the optical band gap due to the quantum confinement effect. These results show clearly that at longer irradiation time, more particles fuse together and form larger particles due to the Ostwald ripening process. The experimental values of the optical band gap are consistent with those obtained from the previous studies.[42]

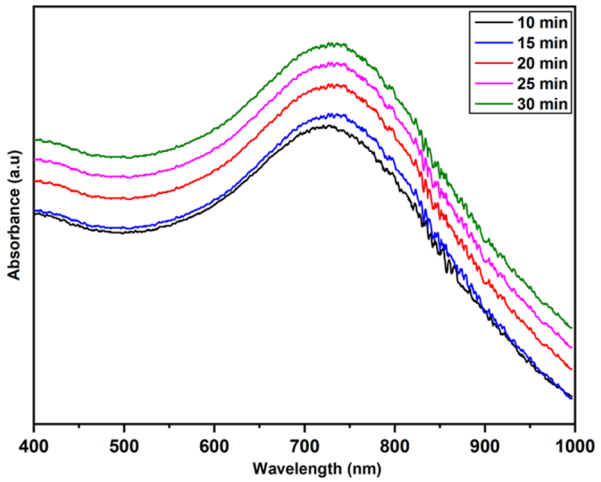

Figure 7. Optical absorption spectra of CuSe NPs at different irradiation times.

Photoluminescence Spectroscopy. Figure 9 shows the room temperature photoluminescence spectroscopy (PL) spectra excited at 400 nm wavelength of CuSe NPs synthesized at different irradiation times via the microwave-assisted method. All the CuSe NP samples have similar PL spectra consisting of two peaks at 525 and 610 nm. The relatively weak green emission observed at 525 nm indicates the existence of intrinsic point defects such as copper vacancies, interstitials, and antisites usually found at the surface of the CuSe NPs. A sharp orange emission observed at 610 nm is attributed to the relaxation of electrons from the conduction band to the valence band of the as-synthesized CuSe NPs. In addition, it is worthy to note that the PL intensity increases as the irradiation time increases, which correlates to the results from the XRD measurement on the enhancement of crystallinity. The optical band gap obtained from the PL spectra is found to be 2.03 eV, which is higher than the value determined from DRS. The higher value of the band gap in the PL measurement could be due to the anti-stoke shifting in CuSe NPs. When a suitable excitation wavelength is used to illuminate a NP, its optical properties can either be detected through elastic (Rayleigh) scattering, where the photons have the energy same as that of the light, or it can be characterized in an inelastic manner, where the photons detected have gained or lost energy to the NPs. If emitted photons are blue-shifted (higher energy), it is typically referred to as anti-stoke shifting, whereas if the photons are red-shifted (lower energy), it is normally referred to as stoke shifting.[43]

CONCLUSIONS

CuSe NPs were successfully synthesized via the microwave-assisted method at different irradiation times. Examination of the XRD patterns shows that the CuSe NPs possess a hexagonal (Klockmannite) crystal structure, while longer irradiation times have led to bigger crystallite sizes. Results from XRD also showed a decrease in the strain and dislocation density in conjunction with the enhancement of the crystallinity of CuSe NPs as the irradiation time increased. This outcome was also corroborated by EDX. Analysis from FESEM and AFM found that the particle grew when the irradiation time was extended with the typical size increasing from 21.15 to 104.89 nm. DRS investigation found that the optical band gap declined from 1.85 to 1.60 eV with longer

https://doi.org/10.1021/acsomega.1c00148
ACS Omega 2021, 6, 10698−10708

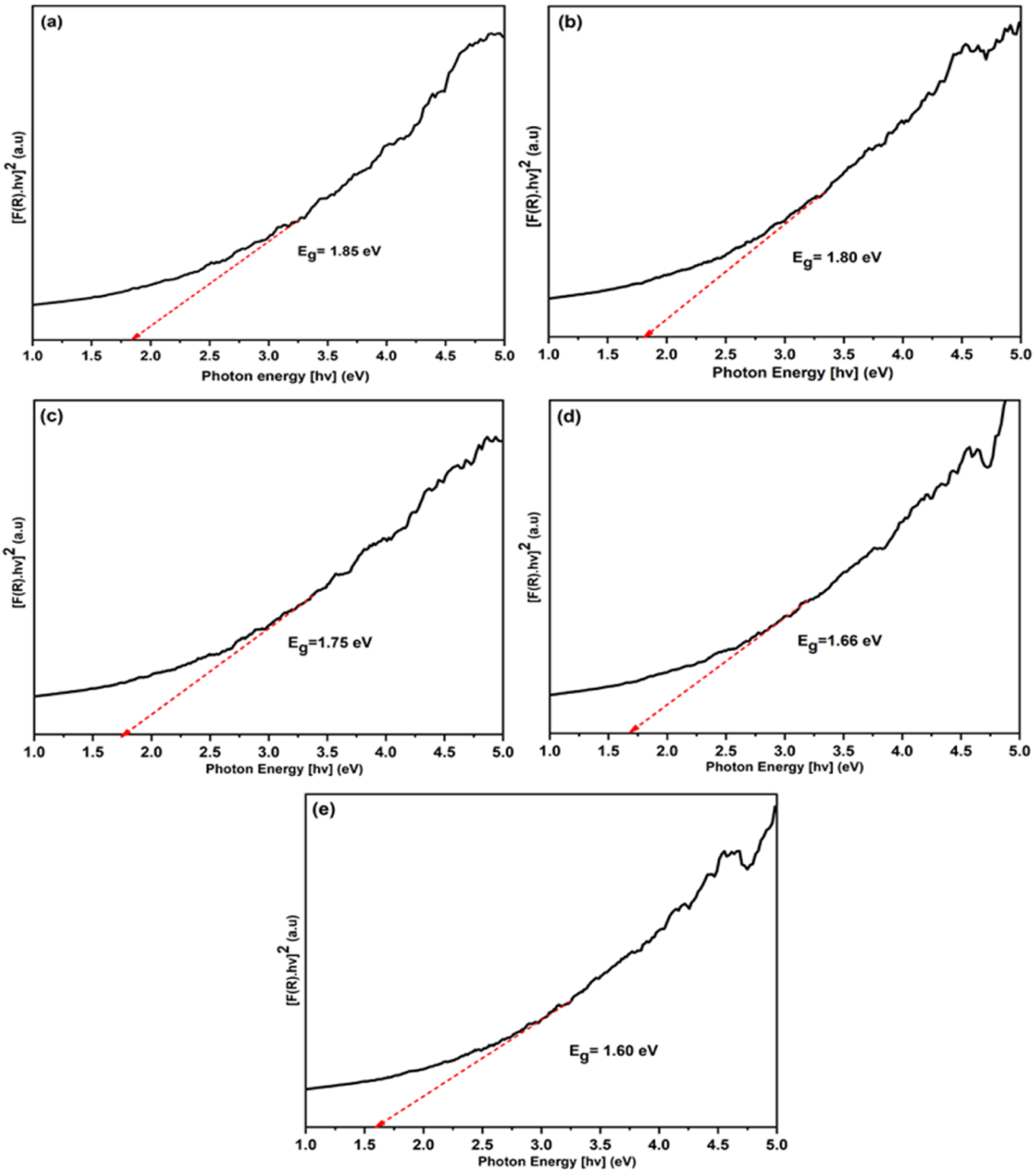

Figure 8. Energy band gap of CuSe NPs at different irradiation times: (a) 10, (b) 15, (c) 20, (d) 25, and (e) 30 min.

Table 3. Particle Size and Their Respective Optical Band Gap of CuSe NPs at Different Irradiation Times

sample designation (min)	particle size (AFM) (nm)	optical band gap (eV)
10	21.15	1.85
15	30.71	1.80
20	32.67	1.75
25	74.16	1.66
30	104.89	1.60

irradiation time. The PL maximum emission of CuSe NPs is centered at 610 nm at 400 nm excitation wavelength, giving an optical band gap value of 2.03 eV. Raman vibrational modes of CuSe NPs were detected at 185.7, 260.2^{-}, and 510.0 cm^{-1} corresponding to the transverse optic (TO), first longitudinal overtone (LO), and second longitudinal overtone (2LO), respectively, of the CuSe NPs. Therefore, the present study illustrates that the irradiation time plays a critical role in shaping the structural and optical characteristics of CuSe NPs synthesized via the microwave-assisted method.

MATERIALS AND METHODS

Materials. The raw materials used in this work are sodium selenide (Na_2SeO_3, purity ≥99% Sigma-Aldrich), hydrazine hydrate ($N_2H_4{\cdot}H_2O$, purity ≥80% Sigma-Aldrich), and copper (II) chloride 2-hydrate ($CuCl_2{\cdot}2H_2O$, purity ≥99% HmBG chemicals). All chemicals were of analytical grade and used without any purification or treatment. Deionized water was used as a solvent.

Experimental Method. The microwave-assisted fabrication of copper selenide nanoparticles (NPs) proceeded as follows: first, a solution of 1.8 mmol (0.3069 ± 0.0002 g) $CuCl_2{\cdot}2H_2O$ dissolved in 50 mL of deionized water was mixed

https://doi.org/10.1021/acsomega.1c00148
ACS Omega 2021, 6, 10698−10708

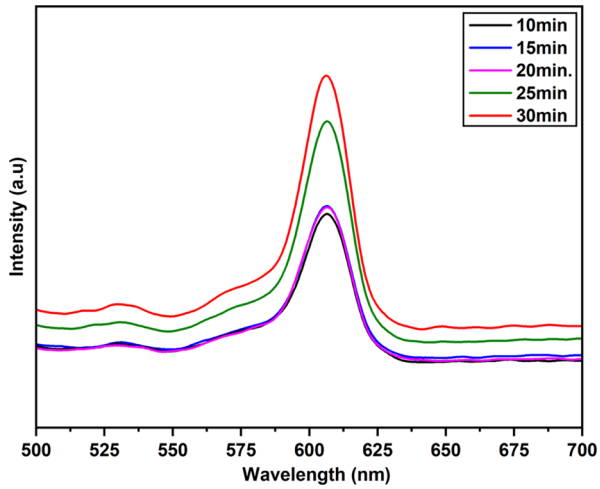

Figure 9. PL spectra of CuSe NPs at different irradiation times.

with a solution containing 2 mmol Na_2SeO_3 (0.3457 ± 0.0002 g) and 3 mL of hydrazine hydrate that were dissolved in 50 mL of deionized water. This resulted in a brown mixture, which was stirred for 5 min at 500 rpm to obtain a homogenous solution. The mixture was then transferred to a microwave oven (Electrolux Microwave Oven ELE-EMM 2001S, 700W) and was irradiated for a specific irradiation time at 380 W microwave power. After the mixture has cooled down to room temperature, it was sonicated for 5 min and centrifuged at 300 rpm several times, first with deionized water and followed with ethanol. The product of the reaction was dried in an oven for 24 h at 60 °C. To determine the role of the irradiation time in the attributes of the synthesized CuSe NPs, the experiment was repeated for the following irradiation times: 10, 15, 20, 25, and 30 min. Figure 10 shows the synthesis process of the CuSe NPs schematically.

Sample Characterization. Study on the phase formation and crystal structure was done by examining the powder X-ray diffraction (PXRD) patterns obtained via an X-ray diffractometer (X'pert Pro, Panalytical) with CuKα radiation (λ = 0.154187 nm). The XRD patterns were measured in the 2θ range of 20−80° and analyzed using X'pert HighScore Plus software. Images of the surfaces of the as-prepared samples were acquired using AFM (Bruker Dimension Edge) with the ScanAsyst peak force tapping mode. The morphology of the as-prepared samples was characterized using a field emission scanning electron microscope (FEI Nova SEM 230) at an accelerating voltage of 10.0 kV and a working distance of 5.2 nm. Elemental analysis of the semiconductor NPs was determined using an EDX spectrometer (7353, Oxford Instruments), while the chemical structure was characterized using Raman spectroscopy (Alpha 300R laser Raman spectrophotometer) measured at 50−1000 cm^{-1}. The optical absorption spectra of the NPs were measured between 400 and 800 nm using a Shimadzu UV−Vis−NIR diffuse reflectance spectrophotometer (Shimadzu-UV3600). The photoluminescence of the NPs was recorded at wavelengths ranging from 500 to 700 nm on a fluoromax3 spectrophotometer (Perkin Elmer LS55) using an excitation wavelength of 400 nm.

AUTHOR INFORMATION

Corresponding Author

Josephine Ying Chyi Liew − *Department of Physics, Faculty of Science and Materials Synthesis and Characterization Laboratory, Institute of Advanced Technology, Universiti Putra Malaysia, 43400 Serdang, Selangor, Malaysia;* orcid.org/0000-0003-1577-4773; Email: josephine@upm.edu.my

Authors

Ibrahim Garba Shitu − *Department of Physics, Faculty of Science, Universiti Putra Malaysia, 43400 Serdang, Selangor, Malaysia; Department of Physics, Faculty of Science, Sule Lamido University, 048 Kafin Hausa, Jigawa State, Nigeria*

Zainal Abidin Talib − *Department of Physics, Faculty of Science, Universiti Putra Malaysia, 43400 Serdang, Selangor, Malaysia; RGS Corporation Sdn Bhd, 43300 Seri Kembangan, Selangor, Malaysia*

Hussein Baqiah − *Department of Physics, Faculty of Science, Universiti Putra Malaysia, 43400 Serdang, Selangor, Malaysia; Shandong Key Laboratory of Biophysics, Institute of Biophysics, Dezhou University, 253023 Dezhou, Shandong, China*

Mohd Mustafa Awang Kechik − *Department of Physics, Faculty of Science, Universiti Putra Malaysia, 43400 Serdang, Selangor, Malaysia*

Mazliana Ahmad Kamarudin − *Department of Physics, Faculty of Science, Universiti Putra Malaysia, 43400 Serdang, Selangor, Malaysia*

Nurul Huda Osman − *Department of Physics, Faculty of Science, Universiti Putra Malaysia, 43400 Serdang, Selangor, Malaysia*

Yiin Jian Low − *Department of Physics, Faculty of Science, Universiti Putra Malaysia, 43400 Serdang, Selangor, Malaysia*

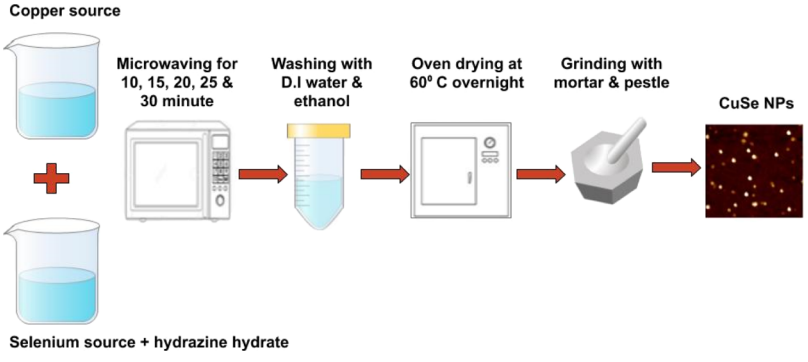

Figure 10. Schematic illustration of the synthesis procedure.

https://doi.org/10.1021/acsomega.1c00148
ACS Omega 2021, 6, 10698−10708

Ismail Ibrahim Lakin − *Department of Physics, Faculty of Science, Universiti Putra Malaysia, 43400 Serdang, Selangor, Malaysia; Department of Physics, Faculty of Science, Kaduna State University, 2339 Tafawa Balewa Way, Kaduna State, Nigeria*

Complete contact information is available at: https://pubs.acs.org/10.1021/acsomega.1c00148

Notes

The authors declare no competing financial interest.

■ ACKNOWLEDGMENTS

The authors would like to acknowledge the support from the Malaysian Ministry of Higher Education for their financial support through (FRGS/1/2018/STG07/UPM/02/5) and Universiti Putra Malaysia through Geran Putra (GPIPS/2018/9664400) and (GP/2018/9618700).

■ REFERENCES

(1) Wu, Y.; Korolkov, I.; Qiao, X.; Zhang, X.; Wan, J.; Fan, X. Facile Synthesis of CuSe Nanoparticles and High-Quality Single-Crystal Two-Dimensional Hexagonal Nanoplatelets with Tunable near-Infrared Optical Absorption. *J. Solid State Chem.* **2016**, *238*, 279−283.

(2) Majima, Y.; Hackenberger, G.; Azuma, Y.; Kano, S.; Matsuzaki, K.; Susaki, T.; Sakamoto, M.; Teranishi, T. Three-Input Gate Logic Circuits on Chemically Assembled Single-Electron Transistors with Organic and Inorganic Hybrid Passivation Layers. *Sci. Technol. Adv. Mater.* **2017**, *18*, 374−380.

(3) Du, P.; Huang, X.; Yu, J. S. Facile synthesis of bifunctional Eu3+-activated NaBiF4 red-emitting nanoparticles for simultaneous white light-emitting diodes and field emission displays. *Chem. Eng. J.* **2018**, *337*, 91−100.

(4) Brahman, P. K.; Suresh, L.; Lokesh, V.; Nizamuddin, S. Fabrication of highly sensitive and selective nanocomposite film based on CuNPs/fullerene-C 60 /MWCNTs: An electrochemical nano-sensor for trace recognition of paracetamol. *Anal. Chim. Acta* **2016**, *917*, 107−116.

(5) Nakata, M.; Zhao, C.; Kanicki, J. DC Sputtered Amorphous In-Sn-Zn-O Thin-Film Transistors: Electrical Properties and Stability. *Solid State Electron.* **2016**, *116*, 22−29.

(6) Pereira, R. N.; Almeida, A. J. Doped Semiconductor Nanoparticles Synthesized in Gas-Phase Plasmas. *J. Phys. D Appl. Phys.* **2015**, *48*, 314005.

(7) Ma, Y.; Ji, H.; Jin, Z.; Wang, J.; Zheng, X.; Yuan, R.; Li, H.; Zhao, S. Hexagonal Plate-Shaped CuSe Nanocrystals by Polylol Solution Chemical Synthesis. *Integr. Ferroelectr.* **2017**, *181*, 102−112.

(8) Xu, J.; Lee, C.-S.; Tang, Y.-B.; Chen, X.; Chen, Z.-H.; Zhang, W.-J.; Lee, S.-T.; Zhang, W.; Yang, Z. Large-scale synthesis and phase transformation of CuSe, CuInSe2, and CuInSe2/CuInS2 core/shell nanowire bundles. *ACS Nano* **2010**, *4*, 1845−1850.

(9) Han, X.; Liao, F.; Zhang, Y.; Yuan, Z.; Chen, H.; Xu, C. CTAB-assisted hydrothermal synthesis of Cu2Se films composed of nanowire networks. *Mater. Lett.* **2018**, *210*, 62−65.

(10) Monjezi, F.; Jamali-sheini, F.; Yousefi, R. Ultrasound-assisted electrodeposition of Cu3Se2 nanosheets and efficient solar cell performance. *J. Alloys Compd.* **2019**, *780*, 626−633.

(11) Giribabu, K.; Suresh, R.; Manigandan, R.; Thirumal, E.; Stephen, A.; Narayanan, V. Aqueous based synthesis of Cu5Se4 nanosheets and characterization. *J. Mater. Sci. Mater. Electron.* **2013**, *24*, 1888−1894.

(12) Urmila, K. S.; Asokan, T. N.; Philip, R. R.; Ganesan, V.; Okram, G. S.; Pradeep, B. Structural, optical, electrical and low temperature thermoelectric properties of degenerate polycrystalline Cu7Se4thin films. *Phys. Status Solidi B* **2014**, *251*, 689−696.

(13) Ghosh, A.; Kulsi, C.; Banerjee, D.; Mondal, A. Galvanic synthesis of Cu 2−X Se thin films and their photocatalytic and thermoelectric properties. *Appl. Surf. Sci.* **2016**, *369*, 525−534.

(14) Shinde, S. K.; Ghodake, G. S.; Dubal, D. P.; Patel, R. V.; Saratale, R. G.; Kim, D.-Y.; Maile, N. C.; Koli, R. R.; Dhaygude, H. D.; Fulari, V. J. Electrochemical synthesis: Monoclinic Cu 2 Se nano-dendrites with high performance for supercapacitors. *J. Taiwan Inst. Chem. Eng.* **2017**, *75*, 271−279.

(15) Hou, X.; Xie, P.; Xue, S.; Feng, H.; Li, L.; Liu, Z.; Zou, R. The Study of Morphology-Controlled Synthesis and the Optical Properties of CuSe Nanoplates Based on the Hydrothermal Method. *Mater. Sci. Semicond. Process.* **2018**, *79*, 92−98.

(16) Singh, V. V.; Singh, A. K. Tetragonal Cu2Se nanoflakes: synthesis using selenated propylamine as Se source and activation of Suzuki and Sonogashira cross coupling reactions. *Dalton Trans.* **2015**, *44*, 725−732.

(17) Garba, I.; Abidin, Z.; Liew, J.; Chi, Y.; Mustapha, M.; Kechick, A.; Baqiah, H. Influence of Tartaric Acid Concentration on Structural and Optical Properties of CuSe Nanoparticles Synthesized via Microwave Assisted Method. *Results Phys.* **2020**, *17*, 103041.

(18) Lala, S.; Maity, T. N.; Singha, M.; Biswas, K.; Pradhan, S. K. Effect of doping (Mg,Mn,Zn) on the microstructure and mechanical properties of spark plasma sintered hydroxyapatites synthesized by mechanical alloying. *Ceram. Int.* **2017**, *43*, 2389−2397.

(19) Lavanya, N.; Anithaa, A. C.; Sekar, C.; Asokan, K.; Bonavita, A.; Donato, N.; Leonardi, S. G.; Neri, G. Effect of Gamma Irradiation on Structural, Electrical and Gas Sensing Properties of Tungsten Oxide Nanoparticles. *J. Alloys Compd.* **2017**, *693*, 366−372.

(20) Shitu, I. G.; Talib, Z. A.; Liew, J. Y. C.; Kechick, M. M. A.; Baqiah, H.; Lee, H. K.; Muhammad, A. Facile Microwave-Assisted Synthesis and Characterization of CuSe Nanosheets: Effect of EDTA Concentration. *J. Mater. Sci. Mater. Electron.* **2020**, *31*, 13549−13560.

(21) Hu, H.; Ge, X.; Deng, C.; Sun, M.; Xuan, H.; Zhang, K. Copper Selenide (CuSe and Cu2Se) Nanocrystals: Controllable Synthesis through a Facile Ultrasonic Chemical Route. *Asian J. Chem.* **2013**, *25*, 5516−5518.

(22) Das, T. R.; Patra, S.; Madhuri, R.; Sharma, P. K. Bismuth Oxide Decorated Graphene Oxide Nanocomposites Synthesized via Sonochemical Assisted Hydrothermal Method for Adsorption of Cationic Organic Dyes. *J. Colloid Interface Sci.* **2018**, *509*, 82−93.

(23) Ansari, F.; Sobhani, A.; Salavati-Niasari, M. Simple sol-gel synthesis and characterization of new CoTiO3/CoFe2O4 nanocomposite by using liquid glucose, maltose and starch as fuel, capping and reducing agents. *J. Colloid Interface Sci.* **2018**, *514*, 723−732.

(24) Rosales, B. A.; Wei, L.; Vela, J. Synthesis and Mixing of Complex Halide Perovskites by Solvent-Free Solid-State Methods. *J. Solid State Chem.* **2019**, *271*, 206−215.

(25) Vinod, T. P.; Jin, X.; Kim, J. Hexagonal Nanoplatelets of CuSe Synthesized through Facile Solution Phase Reaction. *Mater. Res. Bull.* **2011**, *46*, 340−344.

(26) Chikan, V.; McLaurin, E. Rapid Nanoparticle Synthesis by Magnetic and Microwave Heating. *Nanomaterials* **2016**, *6*, 85.

(27) Sanghi, R. Microwave Irradiation. *Resonance* **2000**, *5*, 77−81.

(28) Hussain, R. A.; Hussain, I. Copper Selenide Thin Films from Growth to Applications. *Solid State Sci.* **2020**, *100*, 106101.

(29) Chen, M.; Gao, L. Synthesis and Characterization of Cadmium Selenide Nanorods Via Surfactant-Assisted Hydrothermal Method. *J. Am. Ceram. Soc.* **2005**, *88*, 1643.

(30) Zhang, Q.; Li, H.; Ma, Y.; Zhai, T. ZnSe Nanostructures: Synthesis, Properties and Applications. *Prog. Mater. Sci.* **2016**, *83*, 472−535.

(31) Chen, M.; Gao, L. Synthesis and Characterization of Cadmium Selenide Nanorods via Surfactant-Assisted Hydrothermal Method. *J. Am. Ceram. Soc.* **2005**, *88*, 1643−1646.

(32) Nath, D.; Singh, F.; Das, R. X-ray diffraction analysis by Williamson-Hall, Halder-Wagner and size-strain plot methods of CdSe nanoparticles- a comparative study. *Mater. Chem. Phys.* **2020**, *239*, 122021.

(33) Ilyas, S.; Heryanto, B.; Abdullah, B.; Tahir, D. X-ray diffraction analysis of nanocomposite Fe3O4/activated carbon by Williamson-Hall and size-strain plot methods. *Nano-Struct. Nano-Objects* **2019**, *20*, 100396.

(34) Wasly, H. X-ray Analysis for Determination the Crystallite Size and Lattice Strain in ZnO Nanoparticles. *J. Al-Azhar Univ. Eng. Sect.* **2018**, *13*, 1312−1320.
(35) Pham, N. D.; Tiong, V. T.; Yao, D.; Martens, W.; Guerrero, A.; Bisquert, J.; Wang, H. Guanidinium Thiocyanate Selective Ostwald Ripening Induced Large Grain for High Performance Perovskite Solar Cells. *Nano Energy* **2017**, *41*, 476−487.
(36) Maharaz, M. N.; Halimah, M. K.; Paiman, S.; Saiden, N. M.; Alibe, I. M. Influence of Solvents and Irradiation Time on Structural and Optical Properties of Cubic PbS Nanoparticles. *Int. J. Electrochem. Sci.* **2018**, *13*, 9317−9332.
(37) Kiefer, W. Recent Advances in Linear and Non-Linear Raman Spectroscopy. Part III. *J. Raman Spectrosc.* **2009**, *40*, 1766−1779.
(38) Aydın, Z. Y.; Abacı, S. Synthesis and Characterization of Cu_3Se_2 Nanofilms by an Underpotential Deposition Based Electrochemical Codeposition Technique. *Solid State Sci.* **2017**, *74*, 74−87.
(39) Kubelka, P. New Contributions to the Optics of Intensely Light-Scattering Materials. Part II: Nonhomogeneous Layers*. *J. Opt. Soc. Am.* **1954**, *44*, 330−335.
(40) Fujisawa, J.-i.; Eda, T.; Hanaya, M. Comparative study of conduction-band and valence-band edges of TiO2, SrTiO3, and BaTiO3 by ionization potential measurements. *Chem. Phys. Lett.* **2017**, *685*, 23−26.
(41) Akir, S.; Barras, A.; Coffinier, Y.; Bououdina, M.; Boukherroub, R.; Omrani, A. D. Eco-Friendly Synthesis of ZnO Nanoparticles with Different Morphologies and Their Visible Light Photocatalytic Performance for the Degradation of Rhodamine B. *Ceram. Int.* **2016**, *42*, 10259−10265.
(42) Muthu, S.; Babu Sridharan, M. Synthesis and Characterization of Two Dimensional Copper Selenide (CuSe) Nanosheets. *Mater. Today: Proc.* **2018**, *5*, 23161−23168.
(43) Shinde, K. N.; Dhoble, S. J.; Swart, H. C.; Park, K. Basic Mechanisms of Photoluminescence. *Phosphate Phosphors for Solid-State Lighting*; Springer, 2012; pp 41−59.

https://doi.org/10.1021/acsomega.1c00148
ACS Omega 2021, 6, 10698−10708